Dental Materials Journal 2026; 45(2): 159–168

Development of a bioactive hydroxyapatite concentration gradient double hydroxyapatite/titanium dioxide coating on TiO_2 core block bone

Sang-Hyun CHO[1,2]*, Min-Yong LEE[1]* , Ji-Eun KIM[1]* and Jae-Sung KWON[1,2]

[1] *Department and Research Institute of Dental Biomaterials and Bioengineering, Yonsei University College of Dentistry, Seoul, Republic of Korea*
[2] *BK21 PLUS Project, Yonsei University College of Dentistry, Seoul, Republic of Korea*
Corresponding author, Jae-Sung KWON; E-mail: JKWON@yuhs.ac

There is an increasing demand for bone graft procedures to create sufficient bone volume for implant fixture placement. Among various techniques, block bone grafting is considered a favorable option for both horizontal and vertical augmentation. To meet the required physical and biological characteristics, a novel hydroxyapatite (HA)-coated titanium dioxide (TiO_2) core block bone was developed in this study. The coating layer was designed with an HA concentration gradient to achieve superior compressive strength and wear resistance. The concentration gradient was confirmed by scanning electron microscopy/energy-dispersed X-ray spectroscopy, and coating stability was demonstrated through scratch testing. Furthermore, alizarin red S staining revealed that the HA gradient layer retained bone formation compared to a single-layer HA coating. Taken together, the developed doubled-layered HA gradient TiO_2 block bone shows strong potential as a substitute for conventional block bone grafts.

Keywords: Block bone, Functionally graded materials, Titanium dioxide, Hydroxyapatite

INTRODUCTION

In the surgical field, such as oral and maxillofacial surgery and orthopedics, biomaterials with appropriate mechanical, biocompatibility, and bioactivity are required to reconstruct large bone defects caused by trauma, disease, or surgery[1,2]. The World Health Organization (WHO) predicts that by 2050, approximately 22% of the global population will be aged 60 years or older[3]. This trend of population aging is expected to increase the demand for bone defect reconstruction and dental implants. Consequently, the development of three-dimensional scaffolds that can provide both mechanical reliability and biological functionality has emerged as an important clinical challenge.

Currently, the bone blocks are primarily fabricated from bio-ceramics such as hydroxyapatite (HA) and tricalcium phosphate (TCP), which possess excellent biocompatibility and osteoconductivity[4,5]. Despite their compressive strength, these ceramic-based bone blocks are limited by low toughness and brittleness, making them prone to fracture[6]. To overcome this limitation, previous research has enhanced mechanical reliability and biological activity by incorporating biocompatible metals and polymers[7]. In this study, we addressed these issues by incorporating titanium oxide (TiO_2) into HA through sintering. TiO_2 is not only biocompatible but also has high hardness, appropriate elastic modulus, excellent chemical stability, and strong bone adhesion ability, making it widely used as a dental and orthopedic implant material[7-9]. Sprio *et al.*[10] and Cunha *et al.*[11] reported that TiO_2 not only compensates for the mechanical weakness of HA-based materials but also enhances bioactivity, thereby promising cell adhesion and proliferation. Therefore, the application of this approach to bone blocks is expected to improve both mechanical reliability and biological activity.

Meanwhile, functionally graded materials (FGMs) are structures designed with gradually varying composition and properties[12]. When used as bone substitutes, they can mitigate stress shielding effects and simultaneously ensure mechanical stability and tissue compatibility by adjusting the characteristics of each layer[13]. This structure can maximize the bone response to physiological stress based on Wolff's law. Although several previous studies have explored functionally graded HA/TiO_2 systems, their approaches have largely been limited to creating thin surface coating rather than constructing a truly three-dimensional gradient architecture[14-16]. Moreover, most earlier works focused on either the processing conditions or biological performance alone, lacking an integrated evaluation of thermal optimization, resulting material properties, and osteogenic outcomes.

In contrast, the present study reproduces a millimeter-scale, double-layered gradient structure by mixing HA and TiO_2 at different ratios, followed by controlled sintering to fabricate a bulk FGM bone block. This design enables the simultaneous investigated of three aspects: (i) the optimal sintering temperature for HA/TiO_2 composites, (ii) the corresponding mechanical and surface properties such as compressive strength and scratch resistance, and (iii) the osteogenic differentiation behavior on the graded architecture.

Therefore, this study aims to comprehensively evaluate the physical, mechanical, and biological characteristics of the gradient HA/TiO_2 block and to validate its potential as a next-generation bone-

*These authors contributed equally to this work.
Received Sep 8, 2025: Accepted Dec 2, 2025
doi:10.4012/dmj.2025-222 JOI JST.JSTAGE/dmj/2025-222

regeneration scaffold.

MATERIALS AND METHODS

Size distribution analysis of TiO_2 and HA particles

TiO_2 (Duksan, Ansan, Korea) and HA (OssGen, Daegu, Korea) powders were dispersed in 99% ethanol (Sigma-Aldrich, St. Louis, MO, USA) and sonicated for 10 min to achieve uniform suspension. A small aliquot of each suspension was deposited onto a carbon-coated grid and dried overnight. Particle size analysis of TiO_2 and HA was performed using transmission electron microscopy (TEM; JEM-2100Plus, JEOL, Tokyo, Japan) at ×50,000 magnification. For each material, 50 individual particles were imaged and measured to determine their size distribution.

Optimizing sintering temperature

A homogeneous mixture was prepared by blending 50 wt% HA and 50 wt% TiO_2 using a ball mill (Pulverisette 23, FRITSCH, Idar-Oberstein, Germany). The mixed powder was then subjected to heat treatment in a furnace at 700, 800, 900, 1,000, 1,100, and 1,200ºC (Ceraful-S, AON, Gunpo, Korea). After sintering, the samples were analyzed using Fourier-transform infrared spectroscopy (FTIR), X-ray diffraction (XRD), and scanning electron microscope (SEM).

To examine the influence of sintering temperature on chemical structure and crystallinity, FTIR and XRD analysis were conducted. 1 wt% of the sintered mixture was mixed with 99 wt% potassium bromide (Sigma-Aldrich) and finely ground. The mixture was pressed into pellets and placed in a sample holder for FTIR measurements over the range of 4,000–400 cm^{-1} using an FTIR spectrometer (Vertex 70, Bruker, Billerica, MA, USA). For XRD analysis, phase identification of the sintered was performed using XRD (Ultimate IV, Rigaku, Tokyo, Japan) equipped with a Cu Kα radiation source (λ=1.5406 Å). XRD patterns were collected over a 2θ range 20°–60° at a scanning speed of 1°/min, with an operating voltage of 40 kV, a current of 30 mA, and a step size of 0.02°.

To evaluate microstructural changes with temperature, the morphology of the sintered powders was examined using SEM (IT-500HR, JEOL) at ×1,000 magnification.

For compressive strength testing, cylindrical specimens (4 mm in diameter and 6 mm in height) were fabricated using the same 50 wt% HA/ 50 wt% TiO_2 powder mixture and sintered at 900, 1,000, 1,100, and 1,200°C. Compressive strength was measured using a universal testing machine (UTM; Instron, Norwood, MA, USA) at a crosshead speed of 1 mm/min. Fifteen specimens were tested for each temperature, and the results were analyzed based on 63.2% fracture probability and the corresponding Weibull modulus.

Gradient H/T block specimen preparation

Based on the preceding results, the optimal sintering temperature for the H/T composite was determined to be 1,200ºC. A total of seven groups of specimens were prepared. The general preparation procedure was as follows: powders were placed into a metal mold with a 10 mm diameter, and a uniaxial pressure of 100 MPa was applied for 30 s using a uniaxial press (Model3871, Carver, Wabash, IN, USA). For the pure TiO_2 and pure HA groups, 0.12 g of powder was used.

For the single layer H/T composite blocks (7H3T, 5H5T, and 3H7T), 0.01 g of each H/T powder mixture was first placed into the metal mold and leveled. Subsequently, 0.12 g of TiO_2 powder was added, and the combined powders were compacted. For the functionally graded H/T block specimens (5H/5T-3H/7T and 7H3T-5H5T), 0.01 g of H/T mixture with the higher HA ratio was first placed and lower HA ratio was secondly placed into the mold and leveled. Then, 0.12 g TiO_2 powder was added and pressed.

Evaluating the single and double layer coated block bone using cross-sectional SEM/EDS analysis

The central portions of specimens from all seven groups were sectioned using a high-speed handpiece (Kavo Biberach, Baden-Wurttemberg, Germany). The cut specimens were mounted on cross-sectional holders and examined using SEM. SEM imaging was used to assess defects within the single layer H/T blocks as well as the integrity and continuity of the interfaces between compositional layers in the functionally graded H/T blocks. In addition, energy-dispersive X-ray spectroscopy (EDS; JEOL) was performed to characterize the elemental composition and to evaluate the gradient distribution of titanium, calcium, and phosphorus across the functional gradient H/T blocks.

Surface morphology and roughness

Two specimen samples were prepared for each treatment group. In the non-contact mode, the specimens' surface roughness (R_a) was evaluated using an atomic force microscope (AFM; NX-7, Park Systems, Suwon, Korea). The measured area was 10×10 μm^2. The R_a measurements were obtained in each specimen from five different areas, ensuring each selected area was at least 1 mm apart from the others.

Scratch test

Three specimen samples were prepared for each treatment group. A scratch test was conducted using an ultra-precision surface mechanical analyzer (UNHT3; Anton Paar, Graz, Austria) to evaluate the resistance of each specimen to frictional forces. The indenter was a Rockwell-type with a radius of 100 μm. The initial load was set to 0.01 N, and the final load was set to 10 N. In addition, the indenter loading rate was 20 N/min. A 1 mm scratch was made along the x-axis during the scratch test. For each specimen, scratch tests were conducted in three different areas, with each selected area at least 2 mm apart from the others. This test aimed to determine whether the H/T block was delaminated and measure the depth to which the indenter penetrated the specimen.

Evaluation of cellular attachment and Alizarin Red S (ARS) staining

For the cell attachment analysis, each sample was placed in a 12-well microplate (SPL Life Science, Pocheon, Korea) and subjected to UV sterilization for 30 min. An α-minimum essential (Gibco, Grand Island, NY, USA) growth medium was used to culture an MC3T3 (pre-osteoblast) cell; it was supplemented with 10% fetal bovine serum (FBS; Gibco) and 1% antibiotic-antimycotic (Gibco). Subsequently, 1×10^4 MC3T3-E1 cells were inoculated into each sample and incubated for 7 days. The growth medium was replaced every 2 days. After incubation, the culture medium was aspirated, and the samples were washed twice with Dulbecco's phosphate-buffered saline (DPBS; Gibco). Following the washes, a 4% glutaraldehyde solution (Sigma-Aldrich) was added, and the samples were kept at 4°C for 1 h. For dehydration, the cells were exposed at each step to a series of graded ethanol concentrations (25, 50, 75, and 90%) for 5 min. The plates were then dried overnight at room temperature. The cell attachment was analyzed using an SEM (JEOL) at a magnification of ×1,000.

Differentiation was induced by supplementing the growth medium with 10 mM β-glycerophosphate and 50 μg/mL ascorbic acid to evaluate MC3T3 cell mineralization. The differentiation growth medium was replaced every 2 days, and ARS staining was performed on day 21. Cells were first washed with DPBS and fixed in 70% ethanol at 4°C for 30 min. After fixation, they were washed with distilled water and incubated with 2% ARS solution (pH 4.2) at 37ºC for 2 min. Excess dye was removed by washing, and stained samples were examined at 100× magnification. For quantification, bound ARS was extracted using 10% cetylpyridinium chloride (CPC), and the absorbance was measured at 570 nm. To account for intrinsic ARS affinity of calcium containing specimens, ARS staining and CPC absorbance values from cell-free specimens were compared with those from cell-seeded specimens. All experiments were performed in triplicate.

Statistical analysis

Statistical analysis was performed at $\alpha=0.05$ significance level, and figure error bars represented a 95% confidence interval. SPSS Statistics 23 (IBM, Armonk, NY, USA) was used for the analysis. The Shapiro-Wilk test was used to determine equal variance for all statistical data. One-way analysis of variance (ANOVA) was applied to these values. Tukey's honest significant difference test was used to compare multiple values.

The compressive strength data were arranged in ascending order, and a fracture probability of 63.2% was calculated according to Equation (1), where P_f represents a fracture probability, i signifies the rank when sorted in ascending order, and N denotes the number of specimens. Weibull distribution graphs were generated using OriginPro 8.5 (Microsoft Windows, Redmond, WA, US). The Weibull modulus (m) was determined using Equation (2).

$$P_f=(i-0.5)/N \quad (1)$$

$$\ln\ln[(1/1-P_f)]=m\ln\sigma+b \quad (2)$$

RESULTS

The size distribution analysis of TiO_2 and HA particles

As shown in Fig. 1(a), the HA particles exhibited an average size of 153±44 nm, while the TiO_2 particles in Fig. 1(b) showed a larger average size of 204±51 nm. This difference in particle size between the two powders was statistically significant. Although the size distributions of both HA and TiO_2 powders were non-normal, the modal values of each distribution were clearly distinct, indicating a notable difference in their characteristic particle sizes.

Optimizing sintering temperature

Figure 2(a) presents the FTIR spectra obtained at

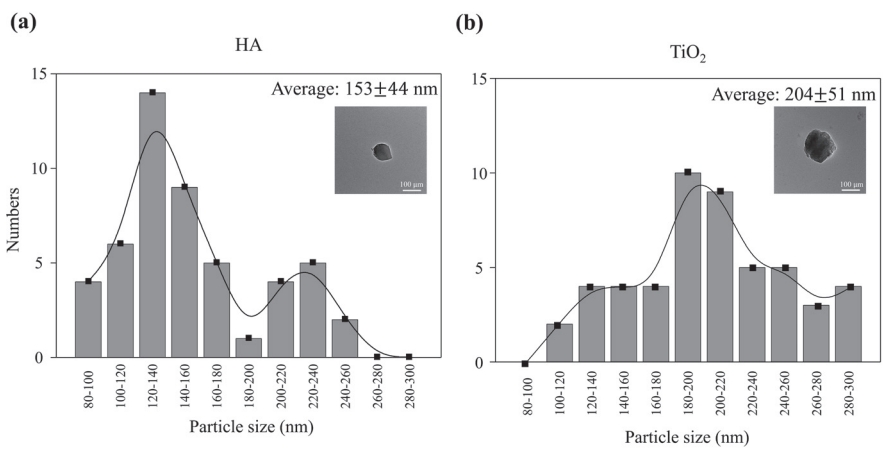

Fig. 1 The particle size distributions and TEM image analyses of HA and TiO_2 powders before mixing.
(a): the particle size distribution of HA; the average of size indicates 153±44 nm, (b): the particle size distribution of TiO_2; the average of size indicates 204±51 nm.

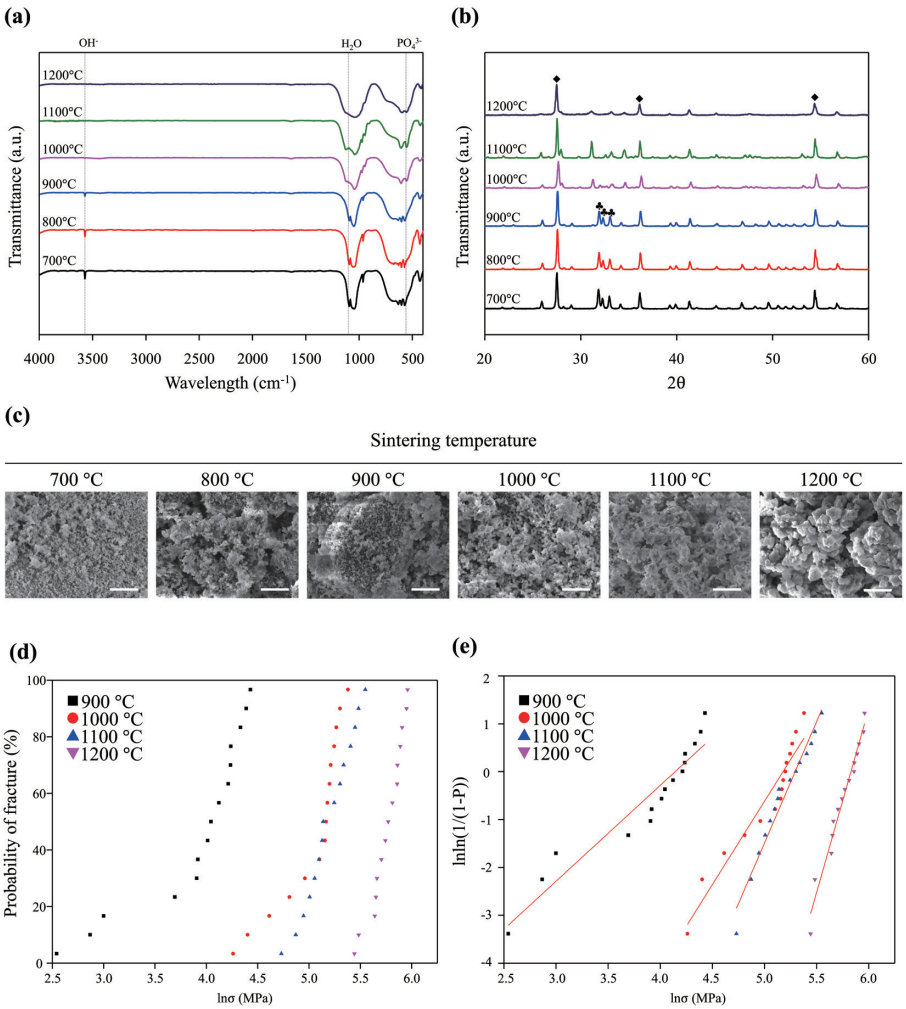

Fig. 2 The analysis of optimizing sintering temperature of 5H5T blocks at different sintering temperatures. (a): FTIR analysis; the peaks of H_2O and OH^- decrease with increasing sintering temperature and the peak of PO_4^{3-} maintains, (b): XRD analysis; Clovers (♣) indicate HA peaks, and diamonds (♦) indicate TiO_2 rutile phase peaks. (c): SEM images; neck formation between particles at temperature above 1,000°C, (d): 63.2% fracture probability of compressive strength and (e): Weibull distribution; mechanical reliability of 5H5T block improves with increasing sintering temperature.

different sintering temperatures. The peak corresponding to the H_2O bending vibration at 1,096 cm^{-1} gradually diminished above 1,000°C and disappeared completely at 1,200°C. Similarly, the OH^- related peak at 3,572 cm^{-1} vanished at temperatures exceeding 1,000°C. In contrast, the PO_4^{3-} peak at 603 cm^{-1} remained consistently detectable across all sintering temperatures.

Figure 2(b) shows the XRD patterns of the samples. New peaks corresponding to β-TCP appeared at 28° and 31.5° at 1,000–1,100°C. However, the characteristic HA peaks at 31.9°, 32.4°, and 33.1° gradually decreased and no longer observed at 1,200°C. By contrast, the rutile phase TiO_2 peaks at 27.39°, 36.09°, and 54.60° were consistently detected at all temperatures, suggesting that no new crystalline phases formed between HA and TiO_2.

Figure 2(c) exhibits SEM images (5,000×) that illustrate the morphological evolution of the H/T composite with sintering temperature. No significant morphological changes were observed between 700 and 900°C. However, above 1,000°C, neck formation between adjacent particles became apparent, leading to reduced porosity and notable densification at ≥1,100°C. At 1,200°C particles exhibited substantial growth and the highest degree of coalescence.

As shown in Fig. 2(d), the Weibull characteristic compressive strength (63.2% fracture probability) increased markedly with temperature, measuring 67.6 MPa at 900°C, 181.3 MPa at 1,000°C, 200.8 MPa at 1,100°C, and 312.4 MPa at 1,200°C. The corresponding Weibull moduli, derived from the linear regression slopes in Fig. 2(e), were 2.00, 3.48, 5.07, and 7.67, respectively, also demonstrating a progressive improvement in mechanical reliability with increasing sintering

temperature.

Collectively, these findings indicate that 1,200°C is the optimal sintering temperature for producing mechanically robust and structurally stable H/T composite materials.

Single and double coating layer analysis

Figure 3 presents SEM cross-sectional images of the fabricated specimen. All specimens showed continuous and well-integrated structures without distinct boundaries between different compositions. Figures 3(a) and (b) display the pure TiO_2 and pure HA blocks, respectively. Figures 3(c)–(e) show single layer H/T block with varying HA ratios, whereas Figs. 3(f) and (g) illustrate the functionally graded double layer coating structures.

As shown in Figs. 3(c)–(e), the Ti atomic percentage gradually increased progressively with decreasing HA content, from 29.85±0.18% in 7H3T, 47.86±0.21% in 5H5T, and 77.55±0.29% in 3H7T. Conversely, the Ca atomic percentage decreased from 42.74±0.19% in 7H3T, 33.08±0.16% in 5H5T, and 13.71±0.11% in 3H7T. In the double layer groups shown in Figs. 3(f) and (g), the EDS mapping confirms a compositional gradient: Ti is enriched near the bottom of the coating and gradually decreased toward the surface in both 5H5T-3H7T and 7H3T-5H5T. Additionally, both the single and double coating layers coatings exhibited uniform thickness, with the single layer coating measuring approximately 75 μm and the double coating measuring approximately 150 μm.

Surface morphology and crystallinity

Figure 4(a) shows representative AFM images for each group. TiO_2 and HA exhibited distinctly different surface morphologies. After sintering, HA showed large grain sizes compared with TiO_2. In addition, the grain size decreased as the TiO_2 content increased in both single and double layer H/T blocks. The functionally graded H/T blocks exhibited grain size patterns similar to those of their corresponding single layer compositions (*e.g.* 5H5T was comparable to 5H5T-3H7T, and 7H3T was

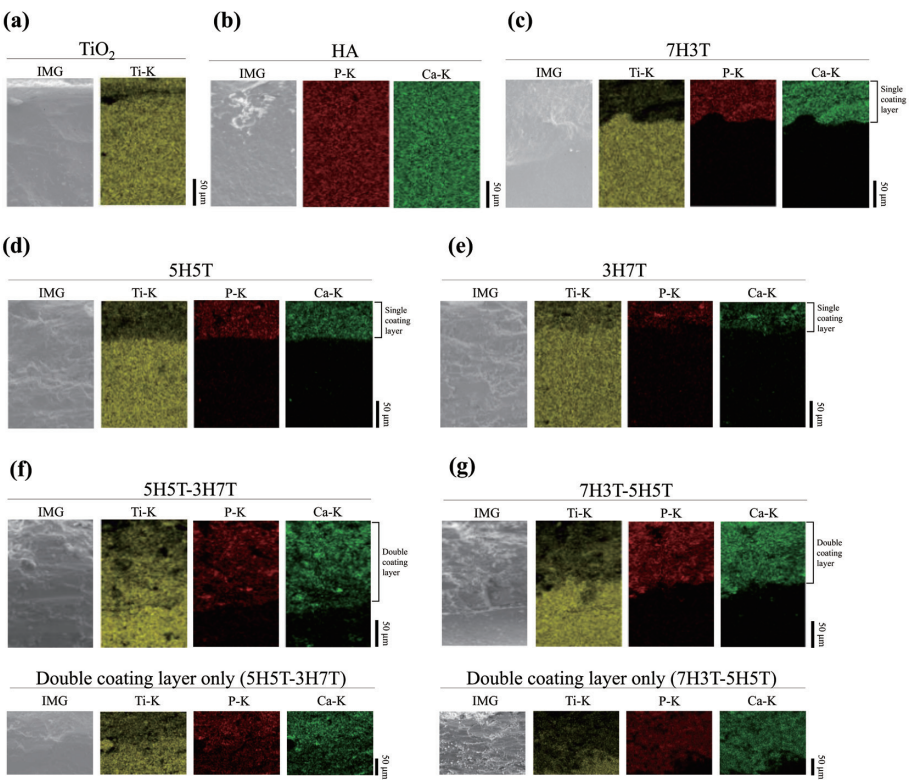

(h)

Single coating layer thickness (μm)			Double coating layer thickness (μm)	
7H3T	5H5T	3H7T	5H5T-3H7T	7H3T-5H5T
77.35±8.67	73.60±4.28	68.12±2.67	157.95±12.39	149.11±10.50

Fig. 3 Single and double coating layer analysis by cross-sectional SEM images and EDS mapping of H/T blocks. The pure blocks; (a): TiO_2, (b): HA, the single layer H/T blocks; (c): 7H3T, (d): 5H5T, (e): 3H7T, the gradient layer H/T block; (f): 5H5T-3H7T, (g): 7H3T-5H5T, (h): coating thickness

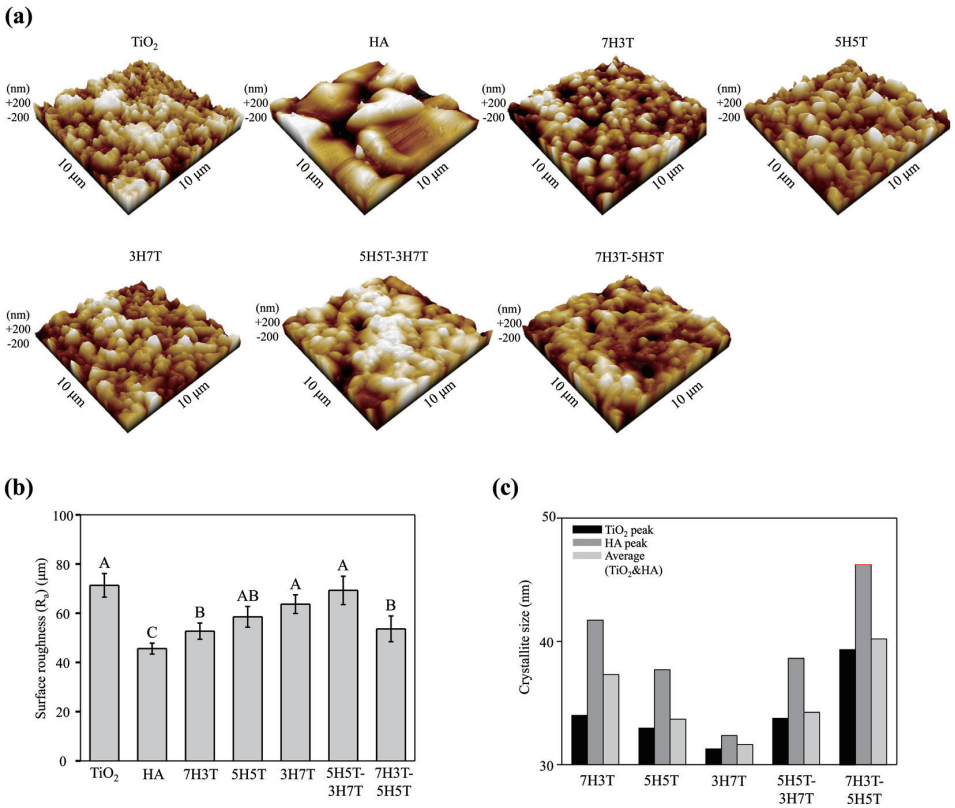

Fig. 4 The analysis of morphology and crystallinity by AFM and XRD of H/T blocks.
(a): AFM image; grain size decreases with increasing the TiO_2 content, (b): Roughness (R_a), R_a increases with increasing TiO_2 content, (c): crystallite size of HA and TiO_2; the crystallite size was analyzed using HA and TiO_2 peaks in the XRD analysis. Letters indicate significant differences of surface roughness at $p<0.05$.

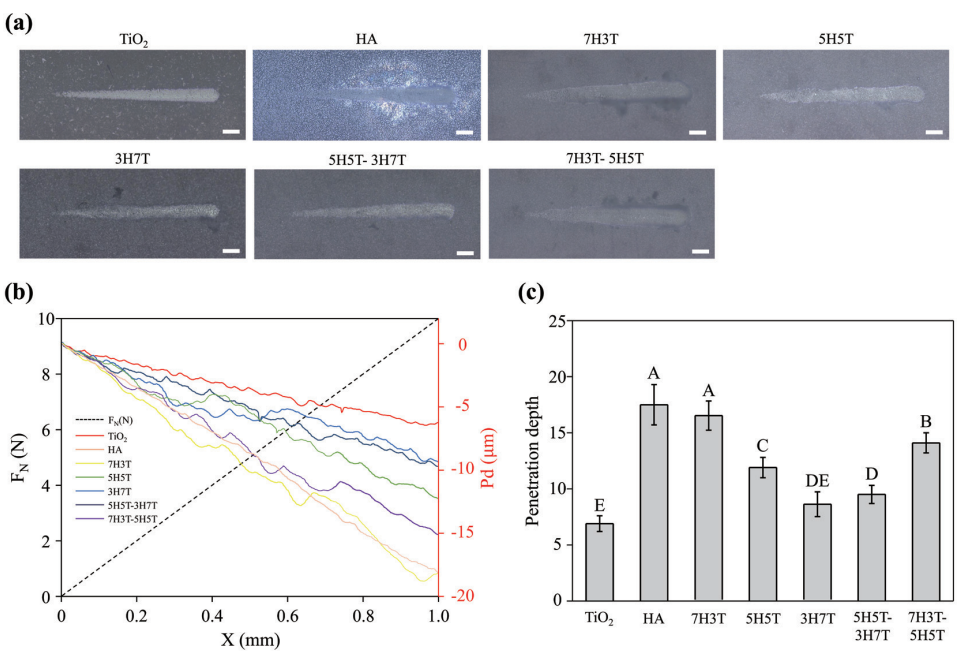

Fig. 5 Scratch test results of H/T blocks.
(a): scratch patterns on the surface, (b): Pd against scratching distance and progressing normal load (F_N), (c): Pd of indenter. Letters indicate significant differences of Pd at $p<0.05$.

comparable to 7H3T-5H5T).

The statistical comparison of surface roughness, shown in Fig. 4(b), indicates that TiO_2 exhibited the highest R_a value (71.346 μm), whereas HA showed the lowest (45.621 μm). Groups with high TiO_2 content—such as 5H5T, 3H7T, and 5H5T-3H7T showed no statistically significant differences in roughness compared with TiO_2. In contrast, 7H3T and 7H3T-5H5T displayed significantly lower roughness than TiO_2 but remained higher than HA.

These roughness trends were closely associated with the crystallinity of each specimen. As shown in Fig. 4(c), higher TiO_2 containing groups (*e.g.*, 3H7T) exhibited lower crystallinity, whereas groups with higher HA content (*e.g.*, 7H3T and 7H3T-5H5T) showed higher crystallinity. Consequently, specimens with higher crystallinity tended to form larger grains, resulting in reduced surface roughness, whereas those with lower crystallinity formed smaller grains, yielding higher roughness.

Scratch test

Figure 5(a) illustrates the typical scratch patterns on the surface of each group. In this test, the penetration depth (Pd) of the indenter into the specimen was measured for each group depending on the magnitude of the friction force applied. The x-axis in Fig. 5(b) represents the distance moved by the indenter, the left y-axis indicates the friction force applied by the indenter, and the right y-axis represents the indenter's Pd. This demonstrates the correlation between each group's representative frictional force and Pd. Figure 5(c) shows the comparison of each group's final Pd values. Generally, the groups with higher TiO_2 contents exhibited lower

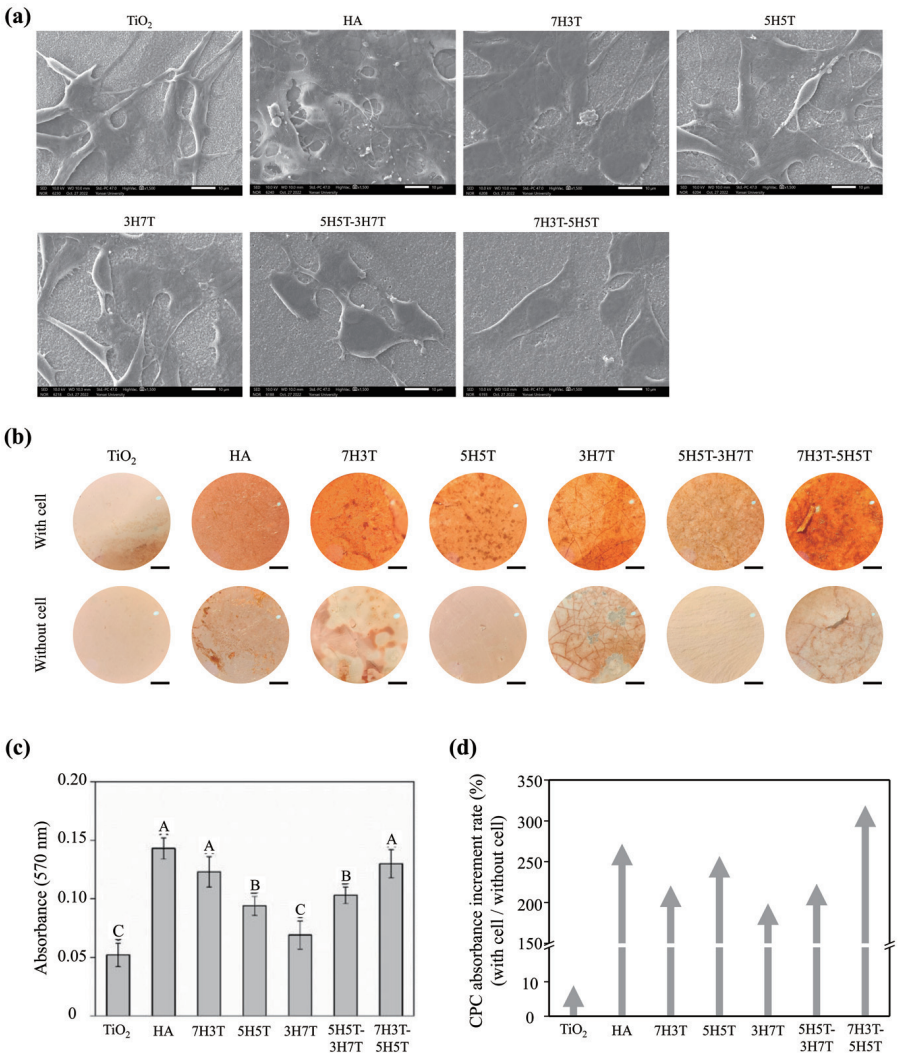

Fig. 6 Evaluation of cellular attachment and ARS of H/T blocks.
(a): SEM images of MC3T3-E1 attachment, (b): ARS analysis for cell differentiation, (c): quantitative analysis of cell differentiation using 100 mM CPC solution, (d): CPC absorbance increment rate (%) of seeded and cell free specimens. Letters indicate significant differences in calcium deposition at $p<0.05$.

Pd values (Pd: TiO_2<3H7T<5H5T<7H3T). Notably, the single H/T block of 5H5T showed a significantly lower Pd than the functional gradient H/Tblock of 5H5T-3H7T. Similarly, 7H3T-5H5T exhibited a statistically lower Pd than 7H3T.

Evaluating cellular attachment and ARS staining

Figure 6(a) shows MC3T3-E1 cell attachment on specimens from each group. Although surface roughness varied among the groups, no significant differences in cellular attachment morphology were observed. Figure 6(b) presents ARS data for specimens with and without cells. As expected, the cell-seeded groups exhibited more intense red staining, indicating greater calcium deposition on the surface.

The CPC-extracted ARS quantification is shown in Fig. 6(c). Groups with higher HA content (*e.g.*, HA, 7H3T, and 7H3T-5H5T) exhibited higher absorbance values, which progressively decreased with increasing TiO_2 content. The CPC absorbance values for the cell-seeded and cell-free specimens are compared in Fig. 6(d). Consistent with the staining images in Fig. 6(b), the cell-seeded specimens demonstrated significantly higher calcium deposition than the cell-free controls.

DISCUSSION

This study expanded the concept of HA-TiO_2 based FGM structures, previously applied to implant coatings[14-16] to a substituted block bone design. Conventional block bone materials exhibit good biocompatibility and osteoconductivity; however, discrepancies in elastic modulus compared with native bone can induce stress shielding, increasing the risk of fracture and reducing new bone formation[12,17-19]. To overcome these limitations, an FGM structure was developed by adjusing the compositional ratio of HA and TiO_2, with the goal of simulatenously improving mechanical stability and biological performance.

Figures 2(a) and (b) demonstrate the chemical structural changes in the HA-TiO_2 (1:1) mixed powder after sintering at various temperatures. At temperatures above 1,000ºC, the OH^- peak of HA were weakened, indicating a phase transformation of HA into TCP due to dehydroxylation. Similar structural transitions have been reported in previous studies and are associated with increased ionic release from calcium phosphate materials. Although HA typically exhibits slow ion release, the disappearance of its characteristic XRD peaks and the emergence of new calcium phosphate phases suggest a potential increase in ion release, which may support enhanced bone formation. Importantly, TiO_2 peaks remained detectable at all sintering temperatures, indicating that TiO_2 was preserved throughout the thermal process and thus contributed to maintaining the mechanical integrity of the composite. Additionally, all experiments shown in Fig. 2 were conducted using powder mixed at a 1:1 HA:TiO_2 ratio to determine the optimal sintering temperature. The purpose of this preliminary test was to evaluate how sintering conditions influence particle fusion, independent of compositional variation. Our results indicated that the HA:TiO_2 ratio did not substantially affect the point at which particle fusion occurred; rather, the sintering temperature was the dominant factor. Therefore, we selected the 1:1 HA:TiO_2 mixture as a representative composition for identifying the optimal sintering temperature and subsequently applied this optimized condition (1,200ºC) to all specimens with varying HA/TiO_2 ratios.

In Fig. 2(c), temperatures above 1,000ºC produced distinct morphological changes: particle boundaries disappeared while pores remained, indicating that the material enterned the densification stage[20]. This suggests that at temperatures above 1,200ºC, HA and TiO_2 can be physically fused. Ceramic-based bone blocks are prone to fracture under external loads due to their brittleness; therefore, ensuring not only mechanical strength but also materials reliability is essential. In this study, the Weibull modulus was analyzed to evaluate the mechanical reliability of bone blocks composed of a 1:1 mixture of HA and TiO_2 at different sintering temperatures. As shown in Fig. 2(e), the slope of the Weibull modulus increased with increasing sintering temperatures, and the bone block sintered at 1,200ºC exhibited the steepest slope, with Weibull modulus of 7.67. This can be attributed to the densification of the bonds between HA and TiO_2 particles with increasing sintering temperatures, which led to an overall increase in density and, consequently, improvements in both compressive strength and fracture resistance. Previous studies reported that the density of HA and TiO_2 sintered at 1,200ºC reached approximately 95% and 96%, respectively, which resulted in improved mechanical strength and reliability[20,21]. Based on the high density and excellent Weibull modulus, the specimens sintered at 1,200ºC were considered to have the highest mechanical reliability. Figure 3 also demonstrates that each block bone possessed a thin and uniform coating layer. Compared with previous studies on HA/TiO_2 FGM structures, the coating layers in this study were thinner, more uniform, and fabricated through a simple process[22,23].

In Fig. 4(c), crystallinity was evaluated by identifying representative diffraction peaks of TiO_2 (27.4º, 36.1º, and 54.3º) and HA (32.4º and 33.0º) and calculating the full width at half maximum (FWHM) for each peak. These FWHM values were then used to determine the relative crystallinity of each specimen. Because grain structure is influenced by crystallinity, the differences in crystallinity among the groups affected their surface roughness. Specimens with lower crystallinity-typically those with higher TiO_2 content-exhibited small grain sizes and higher surface roughness, whereas specimens with higher crystallinity showed larger grains and consequently lower roughness (Fig. 4(b)).

In Figs. 5(b) and (c), the functionally graded H/T block (5H5T-3H7T or 7H3T-5H5T) exhibited a significantly lower Pd compared with 5H5T or 7H3T, consistent with the findings reported by Rezvan Azari *et al.*[16] and Hamidreza Farnoush *et al.*[24] These improvements can be explained by the combined effects

of particle-size refinement and structural stability at the interface. FGMs exhibit enhanced interfacial stability because of the gradual compositional transition between the TiO_2 substrate and the coating layer. For example, compared with the single layer 7H3T, and graded 7H3T-5H5T structure incorporates a 5H5T intermediate layer that acts as a chemical and structural buffer, improving adhesion and mechanical integration with the TiO_2 substrate[25,26]. Furthermore, the FGM structure can mitigate the stiffness mismatch between bone tissue and the bone block by gradually varying the elastic modulus from the core to the surface. Clinically, the elastic modulus of cortical bone ranges from 5 to 23 GPa. Although the elastic modulus of the gradient H/T block was not directly measured in this study, its improved contact behavior suggests that the modulus may be closer to this target range, potentially reducing stiffness mismatch with the surrounding bone tissue.

In Fig. 6(d), the CPC absorbance increase in the TiO_2 group was less than 10%, whereas the other groups showed more than a 200% increase. This indicates that the presence of HA on the surface substantially enhances calcium deposition by MC3T3 cells and promotes their osteogenic differentiation.

This study has several limitations. First, all experiments were conducted *in vitro*. However, *in vivo* environments involve more complex factors such as immune responses, vascularization, and pH fluctuations, which may affect the mechanical performance and biological stability of the gradient H/T block. Second, only short-term analyses of cell adhesion and differentiation were performed. Long-term studies are required to fully evaluate osseointegration and bone formation. Third, the mechanical evaluation was limited to scratch testing, and further assessment of clinically relevant bending strength and fatigue behavior are necessary. Therefore, future studies should include long-term evaluations of the degradation behavior of gradient H/T blocks and the process of bone substitution by cells.

CONCLUSION

This study expanded the concept of HA and TiO_2 based FGM structures, which have mainly been investigated at the coating level in dentistry, by successfully fabricating them into bone blocks. SEM and EDS analyses confirmed that the gradient H/T block exhibited a continuous structure at the interfaces of varying HA and TiO_2 compositions without defects. AFM analysis showed that as the TiO_2 content increased, the crystallite size of the H/T block decreased and the surface roughness increased; however, no significant difference was observed between the single and gradient H/T blocks. In the scratch test, the gradient H/T block demonstrated a significantly lower Pd than the single H/T block due to the stress distribution effect arising from the FGM structure. Furthermore, despite having a higher TiO_2 content, the gradient H/T block maintained a similar level of cell adhesion and differentiation as the single H/T block. Therefore, the gradient H/T block was found to possess superior mechanical and physical strength compared with the single H/T block, while also preserving its biological properties. These findings suggest that gradient H/T blocks hold great promise as biomaterials for bone replacement and reconstruction in dental and orthopedic applications.

ACKNOWLEDGMENTS

This work was supported by the Korea Medical Device Development Fund grant funded by the Korea government (the Ministry of Science and ICT the Ministry of Trade, Industry and Energy, the Ministry of Health & Welfare, the Ministry of Food and Drug Safety) (Project Number: 2470000129, RS-2020-KD000261).

REFERENCES

1) Von Arx T, Buser D. Horizontal ridge augmentation using autogenous block grafts and the guided bone regeneration technique with collagen membranes: A clinical study with 42 patients. Clin Oral Implants Res 2006; 17: 359-366.
2) Degen RM, Camp CL, Werner BC, Dines DM, Dines JS. Trends in bone-block augmentation among recently trained orthopaedic surgeons treating anterior shoulder instability. J Bone Joint Surg 2016; 98: e56.
3) WHO. Ageing and health. 2024; https://www.who.int/news-room/fact-sheets/detail/ageing-and-health
4) Calabrese G, Petralia S, Franco D, Nocito G, Fabbi C, Forte L, *et al.* A new Ag-nanostructured hydroxyapatite porous scaffold: Antibacterial effect and cytotoxicity study. Mater Sci Eng C Mater Biol Appl 2021; 118: 111394.
5) Pearson JJ, Gerken N, Bae C, Lee KB, Satsangi A, McBride S, *et al.* In vivo hydroxyapatite scaffold performance in infected bone defects. J Biomed Mater Res B Appli Biomater 2020; 108: 1157-1166.
6) Vaiani L, Boccaccio A, Uva AE, Palumbo G, Piccininni A, Guglielmi P, *et al.* Ceramic materials for biomedical applications: An overview on properties and fabrication processes. J Funct Biomater 2023; 14: 146.
7) Arab M, Behboodi P, Malek Khachatourian A, Nemati A. Enhanced mechanical properties and biocompatibility of hydroxyapatite scaffolds by magnesium and titanium oxides for bone tissue applications. Heliyon 2024; 10: e33847.
8) Noviyanti AR, Asyiah EN, Permana MD, Dwiyanti D, Suryana, Eddy DR. Preparation of hydroxyapatite-titanium dioxide composite from eggshell by hydrothermal method: Characterization and antibacterial activity. Crystals 2022; 12: 1599.
9) Yin TJ, Steyl SK, Howard J, Carlson K, Jeyapalina S, Naleway SE. Freeze casting of hydroxyapatite-titania composites for bone substitutes. J Biomed Mater Res A 2024; 112: 473-483.
10) Sprio S, Guicciardi S, Dapporto M, Melandri C, Tampieri A. Synthesis and mechanical behavior of β-tricalcium phosphate/titania composites addressed to regeneration of long bone segments. J Mech Behav Biomed Mater 2013; 17: 1-10.
11) Cunha C, Sprio S, Panseri S, Dapporto M, Marcacci M, Tampieri A. High biocompatibility and improved osteogenic potential of novel Ca–P/titania composite scaffolds designed for regeneration of load-bearing segmental bone defects. J Biomed Mater Res A 2013; 101: 1612-1619.
12) Shi H, Zhou P, Li J, Liu C, Wang L. Functional gradient metallic biomaterials: Techniques, current scenery, and future prospects in the biomedical field. Front Bioeng Biotechnol 2020; 8: 616845.
13) Hedia HS, Fouda N. Improved stress shielding on a cementless tibia tray using functionally graded material. Mater Testing

2013; 55: 845-851.
14) Lee JE, Bark CW, Quy HV, Seo SJ, Lim JH, Kang SA, *et al.* Effects of enhanced hydrophilic titanium dioxide-coated hydroxyapatite on bone regeneration in rabbit calvarial defects. Int J Mol Sci 2018; 19: 3640.
15) Rajaeirad M, Fakharifar A, Posti MHZ, Khorsandi M, Watts DC, Elraggal A, *et al.* Evaluating the effect of functionally graded materials on bone remodeling around dental implants. Dent Mater 2024; 40: 858-868.
16) Azari R, Rezaie HR, Khavandi A, Mohammadi EM. Effect of gradient layer of TiO_2-HA on properties of the HA Coated Ti-6Al-4V. Defect Diffus Forum 2020; 400: 193-200.
17) Khaohoen A, Sornsuwan T, Chaijareenont P, Poovarodom P, Rungsiyakull C, Rungsiyakull P. Biomaterials and clinical application of dental implants in relation to bone density—A narrative review. J Clin Med 2023; 12: 6924.
18) Jeong J, Kim JH, Shim JH, Hwang NS, Heo CY. Bioactive calcium phosphate materials and applications in bone regeneration. Biomater Res 2019; 23: 4.
19) Tumedei M, Savadori P, Del Fabbro M. Synthetic blocks for bone regeneration: A systematic review and meta-analysis. Int J Mol Sci 2019; 20: 4221.
20) Trzaskowska M, Vivcharenko V, Przekora A. The impact of hydroxyapatite sintering temperature on its microstructural, mechanical, and biological properties. Int J Mol Sci 2023; 24: 5083.
21) Yan MF, Rhodes WW. Low temperature sintering of TiO_2. Mater Sci Eng 1983; 61: 59-66.
22) Muralithran G, Ramesh S. The effects of sintering temperature on the properties of hydroxyapatite. Ceram Int 2000; 26: 221-230.
23) Qian C, Zhang F, Sun J. Fabrication of Ti/HA composite and functionally graded implant by three-dimensional printing. Biomed Mater Eng 2015; 25: 127-136.
24) Farnoush H, Aghazadeh Mohandesi J, Cimenoglu H. Micro-scratch and corrosion behavior of functionally graded HA-TiO_2 nanostructured composite coatings fabricated by electrophoretic deposition. J Mech Behav Biomed Mater 2015; 46: 31-40.
25) Sukarta IN, Sastrawidana IDK. Synthesis and characterization of hydroxyapatite/titania composite and its application on photocatalytic degradation of remazol Red B textile dye under UV irradiation. Ecol Eng Environ Tech 2024; 25: 178-189.
26) Yılmaz E, Kabataş F, Gökçe A, Fındık F. Production and characterization of a bone-like porous Ti/Ti-hydroxyapatite functionally graded material. J Mater Eng Perform 2020; 29: 6455-6467.